CIGB-300 synthetic peptide, an antagonist of CK2 kinase activity, as a treatment for Covid-19. A computational biology approach

Jamilet Miranda[1*], Ricardo Bringas[1], Jorge Fernández-de-Cossio[1] and Yasser Perera[2,3]

[1]Department of Bioinformatics, Division of Informatics, Center for Genetic Engineering and Biotechnology, Havana, Cuba

[2]Laboratory of Molecular Oncology, Department of Pharmaceuticals, Division of Biomedical Research, Center for Genetic Engineering and Biotechnology, Havana, Cuba

[3]China-Cuba Biotechnology Joint Innovation Center, Yongzhou Zhong Gu Biotechnology Co., Yongzhou, Hunan, People Republic of China

*Corresponding author

E-mail: jamilet.miranda@cigb.edu.cu (JM)

Abstract

Drug repositioning became the first choice for treating Covid-19 patients due to the urgent need to deal with the pandemic. Similarities in the hijacking mechanisms used by SARS-CoV-2 and several type of cancer, suggest the repurposing of cancer drugs to treat Covid-19. CK2 kinase antagonists have been proposed for the treatment of cancer. A recent study in cells infected with SARS-CoV-2 virus found a significant CK2 kinase activity, and the use of a CK2 inhibitor showed antiviral responses. CIGB-300, originally designed as an anticancer peptide, is an antagonist of CK2 kinase activity that binds to CK2 phospho-acceptor sites. Recent preliminary results show an antiviral activity of CIGB-300 versus a surrogate model of coronavirus. Here we present a computational biology study that provides evidences at the molecular level of how CIGB-300 might interfere with SARS-CoV-2 life cycle inside infected human cells. First, from SARS-CoV studies, we infer the potential incidence of CIGB-300 in SARS-CoV-2 interference on immune response. Next, from the analysis of multiple Omics data, we propose the action of CIGB-300 since early stage of viral infections perturbing the virus hijacking of RNA splicing machinery. It was also predicted the interference of CIGB-300 in virus-host interactions responsible for the high infectivity and the particular immune response to SARS-CoV-2 infection. Further, we provide evidences of CIGB-300 attenuation of phenotypes related to muscle, bleeding, coagulation and respiratory disorders.

Introduction

SARS-CoV-2 currently spread world-wide showing high infectivity and transmissibility. Due to the urgency of finding effective therapeutics treatments in the shortest possible time, drug repurposing emerged as the first option [1,2]. The huge amount of data so far generated permit the re-consideration of drugs already evaluated for other diseases, which might have advanced toxicological, preclinical and/or clinical studies.

Since the genomic sequence of SARS-CoV-2 was made available in January 2020 [3], diversity of technique and laboratory models has been profusely applied to the study of SARS-CoV-2 replication and infectivity.

Blanco-Mello et al. [4] performed RNA-seq experiments from polyA RNAs isolated from infected cells. They found a diminished transcriptional response of type I/III interferon-induced genes and, concurrently, a significant increase of chemokines and IL6, which ground their suggestion to evaluate FDA-approved drugs with immunomodulating properties that could be rapidly implemented in clinical protocols.

Various mass-spectrometry studies made important contribution to the comprehension of SARS-CoV-2 life cycle. Gordon et al. [5] using affinity-purification mass spectrometry (AP-MS) identified the sets of human proteins that physically interact with each of 26 viral proteins that they previously individually cloned in human cells derived from kidney HEK-293T/17. A total of 332 physical interactions between SARS-CoV-2 and human proteins were identified. When the expressions of all interacting human proteins in 29 different tissues were analyzed, lung was identified as the one with the highest expression levels. GO enrichment analysis was performed to the set of human

interactors of each viral protein cloned. For each of the 26 sets, the major overrepresented biological processes included Nuclear Transport, Ribonucleoprotein Complex Biogenesis and Cellular Component Disassembly. Host proteins involved in innate immune response were targeted by viral proteins nsp13, nsp15 and orf9b while proteins from the Nf-kB pathway were targeted by nsp13 and orf9c. The most relevant host proteins targeted by known drugs were identified from this analysis. Next, they demonstrated the capacity of some of these drugs to reduce viral infectivity. The study of Gordon et al. [5] is of outstanding relevance for the understanding of the mechanism used by SARS-CoV-2 to improve its infectivity and to avoid a strong immune response. It also provides valuable information for repurposing of existing drugs.

The role of kinases in the course of viral infection was addressed by Bouhaddou et al. [6], who carried a quantitative mass spectrometry-based phosphoproteomics study in Vero E6 cells infected by SARS-CoV-2. Casein kinase II (CK2) and p38 MAP kinases were significantly activated while mitotic kinases were shutdown. A relevant role of CK2 in induced filopodia protrusions during viral infection was evidenced in association with viral capsid protein N. Both CK2 and protein N were co-localized in filopodia protrusions which were significantly longer and more branched than in control cells. The authors suggest that N protein may control CK2 activity and regulate cytoskeleton elements in filopodia. Although the role of CK2 in viral infections is not new, it is remarkable the level of upregulation of CK2 activity as consequence of SARS-CoV-2 infection [6]. The strong antiviral activity of Silmitasertib (CX-4945), a CK2 inhibitor, suggests this kinase as an attractive target for treating Covid-19 patients. Ongoing clinical trial of CX-4945 is

evaluating its clinical benefits and anti-viral activities in moderate COVID-19 patients (https://clinicaltrials.gov/ct2/show/study/NCT04663737).

CIGB-300 is a synthetic peptide designed to bind the phospho-acceptor motif of CK2 substrates, interfering the phosphorylation of serine/threonine residues by CK2. Clinical use of CIGB-300 have confirmed it safety and tolerability when administered intravenously showing clinical efficacy in cancer patients [7,8].

In a phosphoproteomic experiment in NCI-H125 cells, Perera et al. [9] identified CK2 phospho-acceptors peptides that are significantly inhibited by CIGB-300. They found for the first time, that CIGB-300 binds CK2α subunit and impairs CK2α2β2 holoenzyme enzymatic activity. By contrast, phosphorylation of CK2β subunit, which contains itself a consensus CK2 phosphorylation motif, was not influenced by CIGB-300. Additionally, Perera et al. [10] identified nucleophosmin (B23) as a major target of CIGB-300. Of note, Nouri et al. [11] further reported the binding of CIGB-300 to B23 oligomerization domain. This interaction blocks the association of B23 to Rev and US11 proteins, two functionally homologous proteins from HIV and HSV viruses respectively. Cells treated with CIGB-300 showed a significant reduction of virus production suggesting B23 as an attractive target for antiviral drugs. Lobaina and Perera [12] also proposed B23 as a potential target in antiviral therapies.

With this background, CIGB-300 was tested for its safety and clinical benefits in Covid-19 patients in a phase I/II clinical trial [13]. It reduced the number of pulmonary lesions among treated individuals. Additionally, CIGB-300 antiviral effect on MDBK cell infected with bovine coronavirus (BCoV) Mebus was explored [14]. CIGB-300 inhibited the

cytopathic effect and reduced the viral protein accumulation in the cytoplasm. Physical interaction of CIGB-300 with BCoV nucleocapsid protein(N) was also revealed. Functional enrichment found cytoskeleton reorganization and protein folding as the major disturbed biological processes.

Here we present an *in silico* analysis of SARS-CoV and SARS-CoV-2 viral infection. We performed a multi-omics integrative analysis of SARS-CoV-2 infection of human cell lines that combines functional enrichment and network representation. At the level of phosphorylation sites, we integrated data from four different phosphoproteomics studies on SARS-Cov-2 infection [6,15-17] and one study on CIGB-300 inhibition of kinase activity [9]. We identified biological processes and virus activated phosphosites at different times after viral infection that can be interfered by CIGB-300. Our results are consistent with the benefits already evidenced of CIGB-300 treatment in Covid-19 patients.

Results and Discussion

Inferring the potential effect of CIGB-300 treatment on SARS-CoV-2 virus infection based in previous results.

CIGB-300 could alter N-protein localization and its RNA binding capacity

Coronavirus nucleocapsid N proteins play an essential role in virus cell cycle; its dimerization and binding to the viral genomic RNA is the first step for virion particle

assembly. N protein plays an important role in viral genomic RNA synthesis [18] and have been also implicated in the inhibition of type I interferon signaling pathway [19].

A sequence alignment of N protein from SARS-CoV and SARS-CoV-2 viruses show a high similarity (Fig 1). N Protein consists of two structural domains (Fig 1): the N-terminal RNA-binding domain (RBD) (residues 41–186), and the C-terminal dimerization domain (residues 258-361). The rest of the protein is highly disordered [20].

Figure 1: **Sequence alignment of nucleocapside proteins of SARS-CoV-2 (NCAP_SARS2) and SARS-CoV (NCAP_CVHSA) viruses.** Numbers at the right end indicate amino acids position in the SARS-CoV-2 protein. Above the aligned sequences the RNA-binding (residues 41-186, according to UniProt annotation) and Dimerization (residues 258-361) domains are delimited. v-above aminoacid residues indicates phosphorylation sites identified in the works of Davidson et al. [21], Bouhaddou et al. [6], Klann et al. [16] and Hekman et al. [15]. Highlighted are the segment between a CK2 phospho-acceptor site and position +3, in yellow those *in silico* predicted by Surjit et al. [22] and in green those experimentally validated by Davidson et al. [21].

Surjit et al. [22] predicted SARS-CoV N-protein to be heavily phosphorylated. Thr116 and Ser251 were noted as putative phospho-acceptors for CK2 (see Fig 1), though neither has been corroborated experimentally. We collected a total of 33 phosphorylation sites for SARS-CoV-2 N protein (see Fig 1 and S1 Table) from four recent mass spectrometry studies [6,15,16,21] reported two putative CK2 sites at Ser2 and Ser78. Hekman et al. [15] found Ser23 and Ser410 to be phosphorylated by CK2.

Bouhaddou et al. [6] analyzed the impact of phosphorylation in the N-protein surface charges by a 3D structural model of the RNA-binding domain. These changes may modulate the function of N-protein by regulating its RNA binding capacity. One of the phosphorylation sites responsible for these charge changes is the Ser78 (see Fig 1), a CK2 phospho-acceptor site according to Davison et al. [21]. Binding of CIGB-300 to Ser78 would interfere with N-protein RNA binding ability.

On the other hand, N protein is reported to be mainly located in the cytoplasm [22-24]. However, a localization analysis of N-expressing cells treated with four different phosphorylation inhibitors found a significant fraction of N protein localized in the nucleus of cells treated with CDK or CK2 inhibitors [22]. Additionally, in cell infected by BCoV, CIGB-300 bound N protein, downregulated its expression and significantly reduced the accumulation of viral proteins in the cytoplasm [14].

Bouhaddou et al. [6] found CDK activity to be significantly reduced by SARS-CoV-2 infection while CK2 activity is significantly increased. Consequently, inhibition by CIGB-300 of N protein phosphorylation sites may alter, at least in part, its cytoplasmic localization. Hence, the use of CIGB-300 in Covid-19 patients would interfere the N protein role in viral cell cycle in infected cells as its function in particle assembly happens in cytoplasm.

CIGB-300 could bind ORF6 C-terminus and restore IFNs signaling

One important element of innate immune response to virus infections is the activation of antiviral genes as a consequence of interferon production. After activation of receptors by type I interferons, STAT1 is phosphorylated and forms a complex with STAT2 and

IRF9 [25]. This complex exposes a nuclear localization signal (NLS) that is bound by KPNA1, and as a last step before entering the nucleus KPNB1 binds KPNA1 and chaperons the complex through the nuclear pore (Fig 2A) [26].

Figure 2: **Interference of IFN signaling by Orf6 and the role of CIGB-300.** A. Interferon binding to receptor induces STAT1 phosphorylation and formation of a complex with STAT2 and IRF9. KPNA1 binds the complex, KPNB1 binds KPNA1 and chaperons the complex through the nuclear pore. B. Orf6 retains KPNA1 and KPNA2 in the ER/Golgi membrane and the transport of STAT complex to the nucleus interrupted. C. CIGB-300 blocks the interaction of Orf6 with KPNA2 and the transport of STAT complex to the nucleus is restored.

Several groups have attributed an immune response antagonistic effect to Orf6 protein [19,26,27]. In SARS-CoV experiments, Frieman et al. [26] reported that Orf6 interferes with host immune response by antagonizing STAT1 function. Orf6 binds karyopherin alpha 2 (KPNA2) and retains it in the ER/Golgi membrane. KPNB1 is also retained as it binds KPNA2. In this way, the chaperon function of KPNB1 through the nuclear pore is interfered, and STAT1 signaling is interrupted (Fig 2B).

Frieman et al. [26] also found that the C-terminal 10 amino acids of SARS-CoV Orf6 are responsible for KPNA2 binding. In Fig 3 we show the residues of Orf6 involved in the SARS-CoV mutants they generated , $Orf6_{49\text{-}53Ala}$, $Orf6_{54\text{-}58Ala}$ and $Orf6_{59\text{-}63Ala}$ (author's nomenclature), by replacing amino acids 49-53, 54-58 and 59-63 with alanines, respectively. The last two mutants, $Orf6_{54\text{-}58Ala}$ and $Orf6_{59\text{-}63Ala}$, comprising the ten C-

terminal amino acids, did not retain KPNA2 and as consequence, STAT1 function was unaffected. The first mutant $Orf6_{49\text{-}53Ala}$ was still able to retain KPNA2. So, the last ten aminoacids were responsible for KPNA2 binding and, as consequence, for KPNB1 recruitment.

Figure 3: **Sequence alignment of Orf6 proteins of SARS-CoV-2 (NS6_CVHSA) and SARS-CoV-2 (NS6_SARS2) viruses.** Highlighted in red, green and yellow are the residues that were replaced by alanines in the mutants generated by Frieman et al. [26] and Lei et al. [28].

Recently Lei et al. [28] carried a similar mutation study of SARS-CoV-2 Orf6 protein. They generated three different mutants; M1, M2 and M3 (author's nomenclature); by replacing aminoacids 49-52 (YSQL), 53-56 (DEEQ) and 57-61 (PMEID) by alanines, respectively (Orf6 of SARS-CoV-2 lacks the last two amino acids present in SARS-CoV protein). As expected, they obtained similar results: mutant M1 perturbs interferon stimulation as the wild type does, while mutants M2 and M3 lack the inhibitory effect.

In Fig 3 we show an alignment of Orf6 protein sequences from SARS-CoV and SARS-CoV-2 viruses. The region between amino acids 50-53 with the sequence SELD in SARS-CoV protein and sequence SQLD in SARS-CoV-2, both match the CK2 substrate motif. Additionally, this site in SARS-CoV-2 was experimentally found to be phosphorylated, and predicted by computer analysis to be a phospho-acceptor site of CK2 [16]. Ser50, as a CK2 phospho-acceptor site, could be bound by CIGB-300. Mutant M2 of Lei et al. [28] include Asp53 residue at position +3 relative to Ser50, and

this position is known to be important for the recognition of CK2. Therefore, we strongly suggest that the possible binding of CIGB-300 to this phospho-acceptor motif would interfere the interaction of Orf6 C-terminus with KPNA2; avoiding its retention in the ER/Golgi membrane, without interfering KPNA2 chaperon activity of carrying STAT1 complex to the nucleus (Fig 2C). In this regard, CIGB-300 could exhibit an effect that other CK2 antagonists that target CK2 won't.

Interfering NUP98 hijacking by CIGB-300 via interaction with Orf6 C-terminus

We analyzed proteomic expression data from Bojkova et al. [29] and found B23 exhibit the highest positive correlation with the expression profile of viral proteins (S1 Fig). SARS-CoV virus N protein was found to interact with B23 protein [30]. Despite that, Gordon et al. [5] did not reported a direct interaction of B23 with viral proteins. Looking for indirect interactions, we intersected the interactors of B23 with the 322 proteins found by Gordon et al. [5] to interact with viral proteins. A total of 21 host proteins resulted from this intersection, among which Nuclear Pore Complex protein 98 (NUP98) shown up as the only one that interact with Orf6, the viral protein with the highest expression correlation to B23.

Bouhaddou et al. [6] determined that phosphorylation at Ser888 of NUP98 increased during viral infection. The sequence around Ser888 is D**S**DEEE, which fulfills the phospho-acceptor motif of CK2. Additionally, Franchin et al. [31] found the phosphorylation of Ser888 to be altered by a CK2 inhibitor (according to data downloaded from PhosphositePlus web site). NUP98 is part of the Nuclear Pore

Complex, responsible for the transport of biomolecules between the nucleus and cytoplasm. Bouhaddou et al. [6] suggested that the SARS-CoV-2 infection-induced phosphorylation of NUP98 may prevent export of mRNAs through the nuclear pore, a similar mechanism to those used by other viruses to increase the translation of viral RNA in the cytoplasm. Binding of CIGB-300 to Ser888 phospho-acceptor site of NUP98 could prevent its phosphorylation and restore host mRNA translocation to cytoplasm.

Also, Gordon et al. [5] found that Met58 and acidic residues Glu55, Glu59 and Asp61 are highly conserved in Orf6 homologs and are part of a putative NUP98/RAE binding motif. Miorin et al. [32] found that SARS-CoV-2 infection blocks the nuclear translocation of STAT1 and STAT2. Orf6 exerts this anti IFN-I activity by hijacking NUP98. Orf6 directly interact with NUP98 at the Nuclear Pore Complex(NPC) via its C-terminal end. A Met58Arg mutant in Orf6 C-terminal region impairs this interaction and abolish the IFN-I antagonistic effect [32].

The Orf6 interactions with KPNA2 and NUP98 have been both reported to interfere with IFN signaling. In both cases the C-terminal domain of Orf6 was responsible for the interaction, mutations in this region abolished the anti-IFN activity. The binding of CIGB-300 to the CK2 phospho-acceptor site Ser50 in Orf6 could impair the interaction with both KPNA2 and NUP98 and in some extend restore IFN signaling.

CIGB-300 downregulate host proteins phosphosites consistently activated by SARS-CoV-2

We now compare the phosphoproteomics studies of SARS-CoV-2 infection in Vero E6 [6], Caco-2 [16], iAT2 [15] and A549 [17] cell lines with that of Perera et al. [9] on CIGB-300 kinase antagonistic effect in H125.

First, we combined results of the four studies at the level of phosphorylation sites and found a total of 8642 different sites that were upregulated in at least one of the studies (Venn diagram in Fig 4A). As noted by Hekman et al. [15], there are few proteins differentially regulated that coincide in all the four studies. Indeed, we found only six phosphosites that were upregulated by SARS-CoV-2 infection in the four cell lines.

Figure 4: Results of four phosphoproteomics studies on SARS-CoV-infection in iAt2, Vero E6, A549 and Caco-2 cell lines and one study on CIGB-300 treatment effect on phosphorylation in H125 cell line. A. Venn diagram showing unique phosphorylation sites identified as UP regulated in A549, VeroE6, iAT2 and Caco-2 cells. B. Venn diagram showing unique phosphorylation sites identified as UP regulated in A549, VeroE6, iAT2 and Caco-2 cells and DOWN regulated by the action of CIGB-300.

Next, we intersected the data on SARS-CoV-2 infection with that of phosphorylation sites down regulated by the treatment of H125 cell line with CIGB-300, resulting in a total of 364 sites (see Fig 4B). Of the six sites that were found upregulated in the four phosphoproteomics studies, half were downregulated by CIGB-300. These three sites, MATR3_S188, SQSTM1_S272 and DIDO1_S1456, have in common to have tens of

Phosphorylation sites. We envisage that these three phospho-acceptor sites, can be targeted by a CIGB-300 treatment in Covid-19 patients.

MATR3 is a nuclear matrix protein with 36 phosphosites according to UniProt annotations. MATR3 plays multiple functions in DNA/RNA processing, it contains two RNA recognition Motifs and two Zinc Finger domains. It was proposed to stabilize mRNA species, to play a role in the regulation of DNA virus-mediated innate immune response [33] and to be associated to splicing regulation [34]. In HIV-infected cells, Sarracino et al. [35] found MATR3 to be essential for RNA processing. MATR3 phoshorylation was found to greatly enhance its DNA binding ability [36,37]. It is well documented its implications in Amyotrophic lateral sclerosis [38], a disease causing muscle weakness and respiratory failures, symptoms common in Covid-19 patients. CIGB-300 interference on virus-infection induced phosphorylation of MATR3 may play a role diminishing its effects in immune response attenuation and its implications in viral RNA processing.

SQSTM1 exhibit several phosphorylation sites, of these, Ser272 is the only one significantly activated by Sars-CoV-2 in the four phosphoproteomic studies. Zhang et al. [39] found that phosphorylation of SQSTM1 at Thr269 and Ser272 by MAPK13 promotes the microaggregates transport to the microtubule organizing center (MTOC) to form aggresomes which are later degraded through autophagy. Gao et al. [40] also showed that SQSTM1 phosphorylation increases its ability to sequester ubiquitinated proteins into aggresomes playing an important role in aggresome formation. Stukalov et al. [17] revealed significant reduction of autophagy flux by ORF3 which combined with

the augmented microaggregates transport due to SQSTM1 phosphorylation conduces to the accumulation of aggresomes.

Several studies have reported the role of SQSTM1 accumulation and aggresome formation in lung related diseases. Tran et al. [41] demonstrated the role of aggresome formation induced by cigarette smoke in chronic obstructive pulmonary disease (COPD). They found a significant higher accumulation of SQSTM1 in smokers as compared to nonsmokers, and an increased severity of COPD. Wu et al. [42] found that the accumulation of SQSTM1 plays a critical role in airway inflammation induced by nanoparticles.

Cystic fibrosis (CF), is caused by mutations in the gene encoding the cystic fibrosis transmembrane conductance regulator (CFTR), which results in defective autophagy, causing the accumulation of CFTR containing aggregates [43]. SQSTM1 knockdown favoured the clearance of defective CFTR aggregates [44].

Inhibition by CIGB-300 of SQSTM1 phosphorylation at Ser272 may reduce the accumulation of aggresomes and this way attenuates lung inflammation and fibrosis induced by viral infection.

DIDO1 (death inducer-obliterator 1 or death-associated transcription factor DATF1) is a protein involved in apoptosis and have been also implicated in the progression of several type of cancer [45-48]. DIDO1 possess 92 phosphosites, according to data we downloaded from Phosphosite. Of these sites we found 16 that match the CK2 phospho-acceptor motif described by Pinna [49]. It is not clear the implications of DIDO1 in the course of viral infection, but it is known the induction of apoptosis by viral

proteins and then DIDO1 may be activated by apoptosis pathway through phosphorylation. CIGB-300 may interfere this activation.

CIGB-300 at early Stage of SARS_CoV-2 Infection

We examine kinase activity from the earliest stages of the viral infection by analyzing phosphoproteomics data of Bouhaddou et al. [6] at 2h and 4h time points, and from Hekman et al. [15], at 1h and 3h time points.

GSEA analysis with proteins sets ranked by phosphorylation changes was performed to identify enriched REACTOME pathways.

After one hour of infection we observed a clear initial inhibition of host protein synthesis machinery, reflected in the inactivation of several phosphorylation sites of proteins involved in RNA metabolism events, such as “mRNA Splicing” and the “Pre-processing of capped intron containing mRNA” (Fig 5). This inactivation is immediately reverted by the activation of these same biological events at 2h and 3h. Fig 5 show the list of most significant pathways at each time point. The phosphosites listed are of those belonging to proteins from the core enrichment set of each enriched pathway and that were also identified by Perera et al. [9] to be inactivated by CIGB-300. Of those, SRSF1_S199 was the only site to be up-regulated at 2h and 3h. SRSF1_S201 was up-regulated at 3h as well as some other SRSF’s proteins phosphosites (Fig 5).

Figure 5: GSEA gene set enrichment analysis of Reactome pathways of proteins with altered phopsphorylation patterns in iAT2 and Vero cell lines. At the center of

the figure is shown a heat map of the normalized enrichment scores resulted from GSEA analysis. The four columns corresponds to the 1h and 3h time points of iAT2 cell [15] and 2h and 4h time points of Vero cells [6] after infection by SARS-CoV-2. The numbers in small rectangles of the heat map indicate the number of proteins in the enriched set that contain phosphosites upregulated by SARS-CoV-2 infection and inhibited by CIGB-300 [9], these same sites are listed. The Venn diagram in the top right was built for the sets proteins of the “mRNA Splicing” Reactome pathways containing phosphosites that were differentially regulated at 1h, 2h and 3h time points or were inhibited by the action of CIGB-300 according to Perera et al. [9]. The second Venn diagram contains similar information for “Metabolism of RNA” Reactome pathway. All the sites upregulated at some time point by the infection and that were inhibited by CIGB-300 are listed.

SRSFs are RBP splicing factors that belong to the family of S/R rich proteins. Rogan et al. [50] proposed a molecular mechanism for viral-RNA pulmonary infections based on protein expression and RBP binding site pattern analysis. They compared the distribution of RBP binding motifs in several viral genomes including SARS_CoV-2, Influenza A, HIV-1 and Dengue. These authors identified strong RBPs binding sites in SARS-CoV-2 genome. After infection, as the number of SARS-CoV-2 genomes increase, the proportion of SRSFs bound to viral genome versus host transcriptome also increases. As the virus replicates in cytoplasm, newly synthetized SRSF1 molecules are bound by viral RNA and retained there, resulting in the formation of R-loops in the nucleus due to a reduction of RBP import. Rogan et al. [50] suggested that

R-loop induced apoptosis could contribute to the spreading of viral particles to neighboring pneumocytes causing a deterioration of lung functions.

Phosphorylation plays an important role in SRSF proteins function. SRPK1 kinase was shown to phosphorylate multiple serine residues in SR rich domain of SRSF1 [51,52], promoting its nuclear import where it plays an important role in RNA stability [53] and alternative splicing [54]. CK2 was found to be the major kinase that phosphorylate SRPK1 and this phosphorylation occurs mainly at Ser51 and Ser555, resulting in 6-fold activation of the enzyme [55]. After SARS-CoV-2 infection of AT2 cell, Ser51 is activated at 3h and 6h [15].

Fig 6 show the expression profile of CK2 and the levels of phosphorylation of SRPK1 S51 site, according to data from Hekman et al. [15]. A clear correlation is observed between the amount of CK2 kinase and the phosphorylation activation of this phospho-acceptor site, an additional argument supporting the role of CK2 on the activation of SRPK1 during SARS-CoV-2 infection.

Figure 6: CK2 expression and SRKP1_S51 site phosphorylation profiles.

These results are consistent with previous reports predicting an extensive reshaping of splicing pathways by SARS-CoV-2 infection [16,29]. SRSF1 is an important element of this splicing machinery that is clearly used by SARS-CoV-2 for its own replication and translation.

The increasing amount of SRSF1 bound to viral genome as the infection progress is a clear indication of its role in viral RNA processing. Phosphorylation is an important mechanism that control SRSF1 function.

Taking all these together, we suggest that CIGB-300 intervene SRSF1 role in SARS-CoV-2 protein synthesis interfering its phosphorylation by SRPK1 kinase.

Infection-induced protein-protein interactions could be perturbed by CIGB-300

Next, we compared the host-viral PPIs reported by Gordon et al. [5] with phosphoproteomic data from Perera et al. [9] on the identification of CK2 substrates significantly inhibited by the CIGB-300. Fig 7 show virus-host interactions from Gordon et al. [5] in which host proteins contain phospho-acceptor sites that were inhibited by CIGB-300 treatment (highlighted in yellow). In this network several proteins are relate to RNA processing and transcription (LARP1, LARP7, LARP4B), supporting the results already mentioned. Binding of CIGB-300 to phospho-acceptor sites of host proteins inhibiting its phosphorylation may perturb the binding by viral proteins and consequently the viral life cycle.

Figure 7: Viral protein interactions with host proteins with phosphorylation sites inhibited by CIGB-300. Rhombus in red represents viral proteins, rectangles in blue represent host proteins, hexagons represent phospho-acceptor sites. In yellow are shown those sites whose phosphorylation was increased by SARS-CoV-2 infection.

Evaluating how CIGB-300 may interfere host-host protein interactions implicated in virus-induced mechanisms, we found that 68 proteins (SC2_300 set from now on) have activated phospho-acceptor sites in at least two of the four phosphoproteomic studies, which were inhibited by CIGB-300 (see S2 Table). The protein-protein interactions (PPI) network built with these proteins is shown in Fig 8. A majority of the nodes in the network are interconnected indicating potential functional relations among them of biological significance. Proteins are grouped by mRNA metabolism, Cell Cycle, and Selective Autophagy pathways, identified as significant by a Reactome enrichment analysis (see S3 Table). The five proteins with higher degree are also highlighted. Among them are HNRNPA1, HSPB1, SRRM2, and SRRM1, which are implicated in mRNA metabolism, corroborating the potential impact of CIGB-300 in viral replication and transcription. The fifth protein was B23/NPM1, identified as a major target of CIGB-300 in cancer cells, but also as a relevant target for antiviral therapies [10-12].

Figure 8: Interaction network of proteins found to be activated in at least two of the four phosphoproteimics studies analyzed and with phosphoaceptor sites found to be inhibited by the action of CIGB-300. For each protein the phospho-acceptor sites inhibited by CIGB-300 are shown. Proteins involved in more significant pathway are grouped and colored: mRNA metabolism(●), Cell Cycle(●) and 'Selective Autophagy' (●). The five nodes with a higher degree (HNRNPA1, HSPB1, SRRM2, NPM1 and SRRM1) are labeled with (●).

In this network HSPB1 heat shock protein (alias HSP27) is one of the highest degree nodes. HSPB1 was found to be overexpressed in idiopathic pulmonary fibrosis (IPF) patients. It activates pro-fibrotic mechanisms and consequently has been suggested as a target to treat IPF [56,57]. In tumor cells, Ivermectin inhibits the phosphorylation of Ser78 and Ser82 of HSP27, while Ser15 is only slightly inhibited [58]. Also Ivermectin have shown to be on inhibitor of SARS-CoV-2 with a significant reduction of viral RNA levels [59] and increase the clinical recovery of mild and severe Covid-19 patients [60,61]. SARS-CoV-2 activates HSPB1 Ser15 and Ser82 during infection while CIGB-300 inhibits both phospho-acceptor sites [9]. This is an additional argument in favor of using CIGB-300 in Covid-19 patients aiming to reduce pulmonary lesions as it was evidenced in a phase I/II clinical trial [13].

Human phenotypes involving kinase activity induced by SARS-CoV-2, potentially targeted by CIGB-300

We build a network with the top 20 human phenotypes most enriched in the set SC2_300, using GeneCodis tool (see Fig 9 and S4 Table). The network can be divided in two main subnetworks, one related to muscular disorder phenotypes that include Paralysis, Distal muscle weakness, Rimmed Vacuoles, Mildly elevated creatine kinase and Fatigue. The second subnetwork groups phenotypes related to respiratory(Exertional dyspnea, difuse alveolar hemorraghe), bleeding (Metrorrhagia, oral cavity bleeding) and coagulation disorders(Disseminated intravascular coagulation).

Figure 9: **Network representation of Human Phenotypes (HPO) enriched in a set of 68 proteins that contain phospho-acceptor-sites that were activated by SARS-CoV-2 infection in at least two of the four phosphoproteomics studies and inhibited by the action of CIGB-300.** Genecodis functional annotation tool was used for the enrichment analysis and to generate the network of the top 20 enriched phenotypes. Nodes in blue represents enriched phenotypes and nodes in orange represent proteins associated to these phenotypes.

The phenotypes in the first subnetwork are all associated to HNRNPA1, MATR3 and SQSTM1 genes, and have been also reported as Covid-19 symptoms [62-66]. For example, elevated creatine kinase levels is associated to a poor outcome prediction [62] and persistent fatigue is a common symptom in Covid-19 patients [65]. As we mentioned MATR3 and SQSTM1 possess phosphosites that were activated in all four phosphoproteomic studies we analyzed, and HNRNPA1 was the node with the highest degree in the PPI network built. Rimmed Vacuoles, the most significant of the enriched phenotypes, are found in areas of destruction of muscle fibers. Fatigue phenotype is located somewhere in the interface between the two subnetworks and is connected to the three genes mentioned, and also to the three genes that are in the core of the second subnetwork: B23/NPM1, FIP1L1 and NUMA1. The phenotypes in the second subnetwork have been all identified in Covid-19 patients [67,68].

Targeting B23 chaperone activity by CIGB-300

Again B23 surfaced as a relevant player of a viral infection, now in the context of SARS-CoV-2. First, we saw it as the host protein with a higher correlation of expression to

viral proteins, in particular to Orf6. Second, we identified B23 as a highly connected node in a network of proteins consistently upregulated by SARS-CoV-2 infection and inhibited by CIGB-300, which is related to Cell Cycle pathway (Fig 8). Third, it was part of a phenotype network related to respiratory, bleeding and coagulation disorders, symptoms widely reported in Covid-19 disease. Previously, Kondo et al. [69] showed that B23 inhibited the DNA-binding and transcriptional activity of interferon regulatory factor 1(IRF1), while Abe et al. [70] found that B23 regulates the expression of IFN-γ-inducible genes and binds to transcription factors STAT1 and IRF1. Taken together, both Orf6 and B23 might play a role in the inhibitory effect of IFN signaling.

On the other hand, it is known that post- translational modifications like phosphorylation are involved in the regulation of molecular chaperone activities [71]. In particular CK2 phosphorylation was found to play an important role in B23 chaperon activity [72]. CIGB-300 might interfere B23 chaperon activity by inhibiting phosphorylation and perturbing its interactions with host and viral proteins. For instance, Orf6 localize in ER/Golgi membrane and NPC associated to KPNA2 and NUP98, respectively. May B23 chaperone activity play a role in SARS-CoV-2 infected cells by carrying Orf6 to the ER/Golgi membrane and the NPC?

Of note, the CIGB-300 peptide interacted with the B23 protein in MDKB cells infected with a Bovine Coronavirus strain (BCoV) [14]. In these cells, also several host proteins participating in protein folding, populated the interactomic profile of the CIGB-300 peptide. However, to definitively address any particular role of B23/NPM1 in the context of an ongoing coronavirus infection, gain- and/or lost-of-function genetic experiments need to be done.

Conclusion

There is, so far, no definite effective therapeutic treatment against SARS-CoV2, despite progress with the development and extensive use of vaccines. The emergence of increasingly transmissible and aggressive mutated variants of the virus justifies the efforts to find new therapeutics to reduce the ratio of patients that evolve to severe stages and death.

Targeting those mechanisms of host cell that are commonly hijacked by viruses, to reproduce and spread, is a valid strategy to confront present and future challenges of viral epidemics. CK2 kinase activity is activated by multiple viruses and proved to be essential for many virus-induced mechanisms that allow viruses to replicate and damage host cell functions. Phosphorylation is widely altered in human cell immediately after virus entry, contributing to the hijacking of multiple cellular processes.

In this paper putative molecular mechanism are put forward to support the observed antiviral effects of CIGB-300 in coronavirus infections and the preliminary clinical results on preventing virus induced lung injury.

Our *in-silico* analysis provides evidences of the role of CIGB-300 in the reversion, based in CK2 kinase activity inhibition, of virus-induced perturbations of cellular functions such as:

- N protein localization and RNA binding capabilities which are implicated in essential steps of viral life cycle as viral capside assembly.
- Interference of IFN signaling, which is responsible for a weak immune response.

- Early stages of virus kidnapping of RNA processing, which plays an essential role in virus genome replication and translation.

- Aggresome accumulation and its role in Inflammation and fibrosis commonly observed in severe Covid-19 patients.

- Phenotypes related to muscle, bleeding, coagulation and respiratory disorders.

Table 1 summarizes different working hypothesis which need to be verified in suitable pre-clinical models. Notably, while our findings suggest a clear impact of CK2 inhibitors in viral replication and hijacking strategies, differences could be also inferred based on their particular inhibitory mechanism. For instance, the use of CIGB-300 to impair CK2-mediated signaling in cancer do not mirror CX-4945 effects in pre-clinical and clinical settings, thus the same could be expected in viral infections like those caused by coronaviruses. The fact that CIGB-300 targets both the CK2 enzyme and a subset of its substrates, may imply particular inhibitory effects of protein-protein interactions, as well as in the crosstalks with other nearby Post-translational modifications sites [9]; therefore, resulting into different molecular, cellular and organismal outcomes.

Altogether, our computational biology approach supports the potential impact of CIGB-300 in the treatment of Covid-19 patients, and encourages its clinical evaluation from early stages of the viral infection.

537 **Table 1**: **Summary of main findings.**

Analysis Type	Subject	Identity	Working Hypothesis	Experimental Clues	Reference
Individual CK2 sites	Viral proteins	N	CK2 phosphosite inhibition/blockage by CIGB-300 impairs viral replication and IFN signaling	Interaction, co-localization, N mRNA and protein expression inhibition by CIGB-300 in a subrogate model	[14]
Individual CK2 sites	Viral proteins	ORF6	CK2 phosphosite inhibition/blockage by CIGB-300 impairs IFN signaling	Additive/Synergistic profile of CIGB-300 plus IFN alpha	Unpublished
Co-Expression and network propagation	Host and Viral Proteins	NUP98, ORF6, B23	CK2 phosphosite inhibition/blockage by CIGB-300 impairs IFN signaling	Additive/Synergistic profile of CIGB-300 plus IFN alpha (unpublished)	Unpublished
Phosphoproteome overlap	Host Proteins	MATR3, SQSTM1, DIDO1	CIGB-300 Multitarget effect impairing viral transcription/splicing, inflammation, immunoresponse and apoptosis	Pulmonary lesions resolution in CT Phase I	[13]
Kinase activity profiles	Host proteins	SRPK1 (SRSF1,2,6,10)	CIGB-300 impairs Viral RNA splicing	None, to be evaluated in preclincial seetings	NA
PPIs vs H125 Phosphoproteome	Host and Viral Proteins	Several proteins (see text and Fig. 7) [LARP1,LARP7,LARP4B]	CIGB-300 impairs Viral RNA processing and transcription	None, to be evaluated in preclincial seetings	NA
SARS-CoV-2 vs H125 Phosphoproteome overlap, Network and Enrichment analysis	Host proteins	Several proteins (see text and Fig. 8) [HNRNPA1, HSPB1, SRRM2, SRRM1, B23]	CIGB-300 Multitarget effect impairing on mRNA metabolism cell cycle and Autophagy pathways	Pulmonary lesions resolution in CT Phase I	[13]

Human Phenotypes	Host proteins	HNPRNPA1, MATR3, SQSTM1, B23, FIP1L1, NUMA1	CIGB-300 might relief COVID19 clinical symptoms	To be evaluated in CT Phase II	NA

Material and Methods

Public Data

Protein sequence information was downloaded from UniprotKB database [73] https://www.uniprot.org/.

Data sources from phosphoproteomics studies of host and viral proteins of SARS-CoV-2 infected human cell lines were downloaded from site listed in table 2.

Table 2: SARS-CoV-2 infection phosphoproteomics studies data sources.

Reference	Timepoints	Cell lines	Downloaded from:
Bouhaddou et al (2020)	2h,4h,8h,12h and 24h	Vero E6	http://dx.doi.org/10.17632/dpkbh2g9hy.1
Hekman et al (2020)	1h,3h,6h and 24h	iAT2	https://www.ebi.ac.uk/pride/archive/projects/PXD020183
Stukalov et al (2021)	6h and 24h	A549	https://www.nature.com/articles/s41586-021-03493-4#MOESM5
Klann et. al (2020)	24h	CaCo-2	https://www.cell.com/molecular-cell/fulltext/S1097-2765(20)30549-9#supplementaryMaterial

The phosphorylation data of CIGB-300 treatment from Perera et al. [9] were downloaded from https://link.springer.com/article/10.1007%2Fs11010-020-03747-1#additional-information/.

Protein expression data from Bojkova et al. [29] were downloaded from http://corona.papers.biochem2.com/.

A total of 332 humand-SARS-CoV-2 protein-protein interactions from Gordon et al. [5] were downloaded from Biogrid database [74] at https://thebiogrid.org/225737/publication/comparative-host-coronavirus-protein-interaction-networks-reveal-pan-viral-disease-mechanisms.html#!.

Information of CK2 Substrates was downloaded from PhosphoSitePlus at (https://www.phosphosite.org/) [75].

Data Analysis

Sequence alignments were performed with the desktop version of CLUSTALX multiple sequence alignment program [76].

Analysis of proteomics data from Bojkova et al. [29] was carried out with MEV [77]. SAM method [78] for two-class unpaired comparison was used to identify most differentially expressed proteins as implemented in MEV. Parameter delta was set so that the estimated median number of false significant proteins would be cero.

For Bouhaddou et al. [6], Stukalov et al. [17], Klann et al. [16] and Hekman et al. [15] data on phosphorylation induced by SARS-CoV-2 infection, the criteria for choosing differentially phosphorylated sites was $\log_2$ fold change>=0.25 and adjusted-p-value<=0.05, the same values proposed by Hekman et al. [15].

The phosphorylation changes induced by CIGB-300 treatment were extracted from Perera et al. [9] . All inhibitions reported by the authors at 10 and/or 30 minutes were considered.

For Gene Set Enrichment Analysis we used GSEA version 4.1.0 for windows [79,80]. Ordered gene lists for each time point after infection were provided as input. The pre-ranked gene list option was used for databases containing REACTOME and GO biological process gene sets. MSigdb v7.2 gmt files were downloaded from: http://www.gsea-msigdb.org/gsea/downloads.jsp.

Cytoscape tool [81,82] was used to build and merge networks in Figs 7 and 8.

BisoGenet CytoScape plugin [83], available from CytoScape Application Manager, was used to generate Protein- protein interaction (PPI) networks.

Venn Diagrams were generated using web application in http://bioinformatics.psb.ugent.be/.

Functional analysis of enriched pathways and reactions was performed using Reactome Pathway Knowledgebase [84] at: https://reactome.org/. The criteria used for selection was FDR (False Discovery Rate) <=0.05.

GeneCodis 4.0, at https://genecodis.genyo.es/, was used for diseases enrichment analysis [85]. Data sources for Human Phenotypes HPO and OMIM were both consulted individually and integrated. The results were obtained in form of networks clusters.

589 BiNGO plugin [86], available from Cytoscape Application Manager, was used to
590 determine and visualize Gene Ontology (GO) categories statistically overrepresented.

591 Additional statistical analysis and graphs were generated and plotted using GraphPad
592 Prism version 5.00 software (GraphPad Software, San Diego, CA, USA).

593

594 Acknowledgments

595 We thank Ricardo Javier Bringas for the design and drawing of figure 2.

596

597 Author Contributions

598 **Conceptualization:** Jamilet Miranda, Ricardo Bringas, Yasser Perera.
599 **Data curation:** Jamilet Miranda, Ricardo Bringas.
600 **Formal analysis:** Jamilet Miranda, Ricardo Bringas.
601 **Investigation:** Jamilet Miranda, Ricardo Bringas, Yasser Perera.
602 **Methodology:** Jamilet Miranda, Ricardo Bringas, Jorge Fernandez de Cossio, Yasser Perera.
603 **Supervision:** Ricardo Bringas, Yasser Perera.
604 **Writing – original draft:** Jamilet Miranda, Ricardo Bringas.
605 **Writing – review & editing:** Jamilet Miranda, Ricardo Bringas, Jorge Fernandez de Cossio, Yasser
606 Perera.

607

608

References

1. Serafin MB, Bottega A, Foletto VS, da Rosa TF, Horner A, et al. (2020) Drug repositioning is an alternative for the treatment of coronavirus COVID-19. Int J Antimicrob Agents 55: 105969.
2. Zhou Y, Wang F, Tang J, Nussinov R, Cheng F (2020) Artificial intelligence in COVID-19 drug repurposing. Lancet Digit Health 2: e667-e676.
3. Zhou P, Yang XL, Wang XG, Hu B, Zhang L, et al. (2020) A pneumonia outbreak associated with a new coronavirus of probable bat origin. Nature 579: 270-273.
4. Blanco-Melo D, Nilsson-Payant BE, Liu WC, Uhl S, Hoagland D, et al. (2020) Imbalanced Host Response to SARS-CoV-2 Drives Development of COVID-19. Cell 181: 1036-1045 e1039.
5. Gordon DE, Jang GM, Bouhaddou M, Xu J, Obernier K, et al. (2020) A SARS-CoV-2 protein interaction map reveals targets for drug repurposing. Nature 583: 459-468.
6. Bouhaddou M, Memon D, Meyer B, White KM, Rezelj VV, et al. (2020) The Global Phosphorylation Landscape of SARS-CoV-2 Infection. Cell 182: 685-712 e619.
7. Aguila JDFV, Y. G.; Jiménez, R. O. R.; Sacerio, A. L.; Rodríguez, C. R. R.; Fraga, Y. R.; Silva, C. V., (2016) Safety of intravenous application of CIGB-300 in patients with hematological malignancies. EHPMA study. . Revista Cubana de Hematología, Inmunología y Hemoterapia 32: 236-248.
8. García-Diegues RdlT-S, A. (2018) Phase I Study of CIGB-300 Administered Intravenously in Patients with Relapsed/Refractory Solid Tumors. ARCHIVOS DE MEDICINA 1: 4.
9. Perera Y, Ramos Y, Padron G, Caballero E, Guirola O, et al. (2020) CIGB-300 anticancer peptide regulates the protein kinase CK2-dependent phosphoproteome. Mol Cell Biochem 470: 63-75.
10. Perera Y, Farina HG, Gil J, Rodriguez A, Benavent F, et al. (2009) Anticancer peptide CIGB-300 binds to nucleophosmin/B23, impairs its CK2-mediated phosphorylation, and leads to apoptosis through its nucleolar disassembly activity. Mol Cancer Ther 8: 1189-1196.
11. Nouri K, Moll JM, Milroy LG, Hain A, Dvorsky R, et al. (2015) Biophysical Characterization of Nucleophosmin Interactions with Human Immunodeficiency Virus Rev and Herpes Simplex Virus US11. PLoS One 10: e0143634.
12. Lobaina Y, Perera Y (2019) Implication of B23/NPM1 in Viral Infections, Potential Uses of B23/NPM1 Inhibitors as Antiviral Therapy. Infect Disord Drug Targets 19: 2-16.
13. Cruz LR, Baladron I, Rittoles A, Diaz PA, Valenzuela C, et al. (2020) Treatment with an Anti-CK2 Synthetic Peptide Improves Clinical Response in COVID-19 Patients with Pneumonia. A Randomized and Controlled Clinical Trial. ACS Pharmacol Transl Sci 4: 206-212.
14. Ramón A, Pérez G, Caballero E, Rosales M, Aguilar D, et al. (2021) Targeting of Protein Kinase CK2 Elicits Antiviral Activity on Bovine Coronavirus Infection.
15. Hekman RM, Hume AJ, Goel RK, Abo KM, Huang J, et al. (2020) Actionable Cytopathogenic Host Responses of Human Alveolar Type 2 Cells to SARS-CoV-2. Mol Cell 80: 1104-1122 e1109.
16. Klann K, Bojkova D, Tascher G, Ciesek S, Munch C, et al. (2020) Growth Factor Receptor Signaling Inhibition Prevents SARS-CoV-2 Replication. Mol Cell 80: 164-174 e164.
17. Stukalov A, Girault V, Grass V, Karayel O, Bergant V, et al. (2021) Multilevel proteomics reveals host perturbations by SARS-CoV-2 and SARS-CoV. Nature 594: 246-252.
18. Wu CH, Chen PJ, Yeh SH (2014) Nucleocapsid phosphorylation and RNA helicase DDX1 recruitment enables coronavirus transition from discontinuous to continuous transcription. Cell Host Microbe 16: 462-472.
19. Li JY, Liao CH, Wang Q, Tan YJ, Luo R, et al. (2020) The ORF6, ORF8 and nucleocapsid proteins of SARS-CoV-2 inhibit type I interferon signaling pathway. Virus Res 286: 198074.

20. Chang CK, Sue SC, Yu TH, Hsieh CM, Tsai CK, et al. (2006) Modular organization of SARS coronavirus nucleocapsid protein. J Biomed Sci 13: 59-72.
21. Davidson AD, Williamson MK, Lewis S, Shoemark D, Carroll MW, et al. (2020) Characterisation of the transcriptome and proteome of SARS-CoV-2 reveals a cell passage induced in-frame deletion of the furin-like cleavage site from the spike glycoprotein. Genome Med 12: 68.
22. Surjit M, Kumar R, Mishra RN, Reddy MK, Chow VT, et al. (2005) The severe acute respiratory syndrome coronavirus nucleocapsid protein is phosphorylated and localizes in the cytoplasm by 14-3-3-mediated translocation. J Virol 79: 11476-11486.
23. Chang MS, Lu YT, Ho ST, Wu CC, Wei TY, et al. (2004) Antibody detection of SARS-CoV spike and nucleocapsid protein. Biochem Biophys Res Commun 314: 931-936.
24. Zhang J, Cruz-Cosme R, Zhuang MW, Liu D, Liu Y, et al. (2020) A systemic and molecular study of subcellular localization of SARS-CoV-2 proteins. Signal Transduct Target Ther 5: 269.
25. Schneider WM, Chevillotte MD, Rice CM (2014) Interferon-stimulated genes: a complex web of host defenses. Annu Rev Immunol 32: 513-545.
26. Frieman M, Yount B, Heise M, Kopecky-Bromberg SA, Palese P, et al. (2007) Severe acute respiratory syndrome coronavirus ORF6 antagonizes STAT1 function by sequestering nuclear import factors on the rough endoplasmic reticulum/Golgi membrane. J Virol 81: 9812-9824.
27. Yuen CK, Lam JY, Wong WM, Mak LF, Wang X, et al. (2020) SARS-CoV-2 nsp13, nsp14, nsp15 and orf6 function as potent interferon antagonists. Emerg Microbes Infect 9: 1418-1428.
28. Lei X, Dong X, Ma R, Wang W, Xiao X, et al. (2020) Activation and evasion of type I interferon responses by SARS-CoV-2. Nat Commun 11: 3810.
29. Bojkova D, Klann K, Koch B, Widera M, Krause D, et al. (2020) Proteomics of SARS-CoV-2-infected host cells reveals therapy targets. Nature 583: 469-472.
30. Zeng Y, Ye L, Zhu S, Zheng H, Zhao P, et al. (2008) The nucleocapsid protein of SARS-associated coronavirus inhibits B23 phosphorylation. Biochem Biophys Res Commun 369: 287-291.
31. Franchin C, Cesaro L, Salvi M, Millioni R, Iori E, et al. (2015) Quantitative analysis of a phosphoproteome readily altered by the protein kinase CK2 inhibitor quinalizarin in HEK-293T cells. Biochim Biophys Acta 1854: 609-623.
32. Miorin L, Kehrer T, Sanchez-Aparicio MT, Zhang K, Cohen P, et al. (2020) SARS-CoV-2 Orf6 hijacks Nup98 to block STAT nuclear import and antagonize interferon signaling. Proc Natl Acad Sci U S A 117: 28344-28354.
33. Salton M, Elkon R, Borodina T, Davydov A, Yaspo ML, et al. (2011) Matrin 3 binds and stabilizes mRNA. PLoS One 6: e23882.
34. Yamaguchi A, Takanashi K (2016) FUS interacts with nuclear matrix-associated protein SAFB1 as well as Matrin3 to regulate splicing and ligand-mediated transcription. Sci Rep 6: 35195.
35. Sarracino A, Gharu L, Kula A, Pasternak AO, Avettand-Fenoel V, et al. (2018) Posttranscriptional Regulation of HIV-1 Gene Expression during Replication and Reactivation from Latency by Nuclear Matrix Protein MATR3. mBio 9.
36. Hibino Y, Ohzeki H, Hirose N, Sugano N (1998) Involvement of phosphorylation in binding of nuclear scaffold proteins from rat liver to a highly repetitive DNA component. Biochim Biophys Acta 1396: 88-96.
37. Malik AM, Barmada SJ (2021) Matrin 3 in neuromuscular disease: physiology and pathophysiology. JCI Insight 6.
38. Johnson JO, Pioro EP, Boehringer A, Chia R, Feit H, et al. (2014) Mutations in the Matrin 3 gene cause familial amyotrophic lateral sclerosis. Nat Neurosci 17: 664-666.
39. Zhang C, Gao J, Li M, Deng Y, Jiang C (2018) p38delta MAPK regulates aggresome biogenesis by phosphorylating SQSTM1 in response to proteasomal stress. J Cell Sci 131.

40. Gao J, Li M, Qin S, Zhang T, Jiang S, et al. (2016) Cytosolic PINK1 promotes the targeting of ubiquitinated proteins to the aggresome-autophagy pathway during proteasomal stress. Autophagy 12: 632-647.
41. Tran I, Ji C, Ni I, Min T, Tang D, et al. (2015) Role of Cigarette Smoke-Induced Aggresome Formation in Chronic Obstructive Pulmonary Disease-Emphysema Pathogenesis. Am J Respir Cell Mol Biol 53: 159-173.
42. Wu Y, Jin Y, Sun T, Zhu P, Li J, et al. (2020) p62/SQSTM1 accumulation due to degradation inhibition and transcriptional activation plays a critical role in silica nanoparticle-induced airway inflammation via NF-kappaB activation. J Nanobiotechnology 18: 77.
43. Luciani A, Villella VR, Esposito S, Brunetti-Pierri N, Medina DL, et al. (2011) Cystic fibrosis: a disorder with defective autophagy. Autophagy 7: 104-106.
44. Luciani A, Villella VR, Esposito S, Brunetti-Pierri N, Medina D, et al. (2010) Defective CFTR induces aggresome formation and lung inflammation in cystic fibrosis through ROS-mediated autophagy inhibition. Nat Cell Biol 12: 863-875.
45. Garcia-Domingo D, Leonardo E, Grandien A, Martinez P, Albar JP, et al. (1999) DIO-1 is a gene involved in onset of apoptosis in vitro, whose misexpression disrupts limb development. Proc Natl Acad Sci U S A 96: 7992-7997.
46. Lerebours F, Vacher S, Guinebretiere JM, Rondeau S, Caly M, et al. (2021) Hemoglobin overexpression and splice signature as new features of inflammatory breast cancer? J Adv Res 28: 77-85.
47. Li J, Wang AS, Wang S, Wang CY, Xue S, et al. (2020) Death-inducer obliterator 1 (DIDO1) silencing suppresses growth of bladder cancer cells through decreasing SAPK/JNK signaling cascades. Neoplasma 67: 1074-1084.
48. Xiao J, Zhang R, Peng J, Yang Z (2020) BAP1 maintains chromosome stability by stabilizing DIDO1 in renal cell carcinoma. Am J Cancer Res 10: 1455-1466.
49. Pinna LA (2002) Protein kinase CK2: a challenge to canons. J Cell Sci 115: 3873-3878.
50. Rogan PA-O, Mucaki EJ, Shirley BC (2021) A proposed molecular mechanism for pathogenesis of severe RNA-viral pulmonary infections.
51. Hagopian JC, Ma CT, Meade BR, Albuquerque CP, Ngo JC, et al. (2008) Adaptable molecular interactions guide phosphorylation of the SR protein ASF/SF2 by SRPK1. J Mol Biol 382: 894-909.
52. Mole S, Faizo AAA, Hernandez-Lopez H, Griffiths M, Stevenson A, et al. (2020) Human papillomavirus type 16 infection activates the host serine arginine protein kinase 1 (SRPK1) - splicing factor axis. J Gen Virol 101: 523-532.
53. Li X, Manley JL (2005) Inactivation of the SR protein splicing factor ASF/SF2 results in genomic instability. Cell 122: 365-378.
54. Ghosh G, Adams JA (2011) Phosphorylation mechanism and structure of serine-arginine protein kinases. FEBS J 278: 587-597.
55. Mylonis I, Giannakouros T (2003) Protein kinase CK2 phosphorylates and activates the SR protein-specific kinase 1. Biochem Biophys Res Commun 301: 650-656.
56. Park AM, Kanai K, Itoh T, Sato T, Tsukui T, et al. (2016) Heat Shock Protein 27 Plays a Pivotal Role in Myofibroblast Differentiation and in the Development of Bleomycin-Induced Pulmonary Fibrosis. PLoS One 11: e0148998.
57. Wettstein G, Bellaye PS, Kolb M, Hammann A, Crestani B, et al. (2013) Inhibition of HSP27 blocks fibrosis development and EMT features by promoting Snail degradation. FASEB J 27: 1549-1560.
58. Nappi L, Aguda AH, Nakouzi NA, Lelj-Garolla B, Beraldi E, et al. (2020) Ivermectin inhibits HSP27 and potentiates efficacy of oncogene targeting in tumor models. J Clin Invest 130: 699-714.
59. Caly L, Druce JD, Catton MG, Jans DA, Wagstaff KM (2020) The FDA-approved drug ivermectin inhibits the replication of SARS-CoV-2 in vitro. Antiviral Res 178: 104787.

748 60. Ahmed S, Karim MM, Ross AG, Hossain MS, Clemens JD, et al. (2021) A five-day course of ivermectin
749 for the treatment of COVID-19 may reduce the duration of illness. Int J Infect Dis 103: 214-216.
750 61. Okumus N, Demirturk N, Cetinkaya RA, Guner R, Avci IY, et al. (2021) Evaluation of the effectiveness
751 and safety of adding ivermectin to treatment in severe COVID-19 patients. BMC Infect Dis 21:
752 411.
753 62. Akbar MR, Pranata R, Wibowo A, Lim MA, Sihite TA, et al. (2021) The prognostic value of elevated
754 creatine kinase to predict poor outcome in patients with COVID-19 - A systematic review and
755 meta-analysis. Diabetes Metab Syndr 15: 529-534.
756 63. Chan KH, Farouji I, Abu Hanoud A, Slim J (2020) Weakness and elevated creatinine kinase as the
757 initial presentation of coronavirus disease 2019 (COVID-19). Am J Emerg Med 38: 1548 e1541-
758 1548 e1543.
759 64. De Giorgio MR, Di Noia S, Morciano C, Conte D (2020) The impact of SARS-CoV-2 on skeletal muscles.
760 Acta Myol 39: 307-312.
761 65. Townsend L, Dyer AH, Jones K, Dunne J, Mooney A, et al. (2020) Persistent fatigue following SARS-
762 CoV-2 infection is common and independent of severity of initial infection. PLoS One 15:
763 e0240784.
764 66. Versace V, Sebastianelli L, Ferrazzoli D, Saltuari L, Kofler M, et al. (2021) Case Report: Myopathy in
765 Critically Ill COVID-19 Patients: A Consequence of Hyperinflammation? Front Neurol 12: 625144.
766 67. Levi M, Iba T (2021) COVID-19 coagulopathy: is it disseminated intravascular coagulation? Intern
767 Emerg Med 16: 309-312.
768 68. Singh P, Schwartz RA (2020) Disseminated intravascular coagulation: A devastating systemic disorder
769 of special concern with COVID-19. Dermatol Ther 33: e14053.
770 69. Kondo T, Minamino N, Nagamura-Inoue T, Matsumoto M, Taniguchi T, et al. (1997) Identification
771 and characterization of nucleophosmin/B23/numatrin which binds the anti-oncogenic
772 transcription factor IRF-1 and manifests oncogenic activity. Oncogene 15: 1275-1281.
773 70. Abe M, Lin J, Nagata K, Okuwaki M (2018) Selective regulation of type II interferon-inducible genes
774 by NPM1/nucleophosmin. FEBS Lett 592: 244-255.
775 71. Jovcevski B, Kelly MA, Rote AP, Berg T, Gastall HY, et al. (2015) Phosphomimics destabilize Hsp27
776 oligomeric assemblies and enhance chaperone activity. Chem Biol 22: 186-195.
777 72. Szebeni A, Hingorani K, Negi S, Olson MO (2003) Role of protein kinase CK2 phosphorylation in the
778 molecular chaperone activity of nucleolar protein b23. J Biol Chem 278: 9107-9115.
779 73. Pundir S, Martin MJ, O'Donovan C (2017) UniProt Protein Knowledgebase. Methods Mol Biol 1558:
780 41-55.
781 74. Stark C, Breitkreutz BJ, Reguly T, Boucher L, Breitkreutz A, et al. (2006) BioGRID: a general repository
782 for interaction datasets. Nucleic Acids Res 34: D535-539.
783 75. Hornbeck PV, Zhang B, Murray B, Kornhauser JM, Latham V, et al. PhosphoSitePlus, 2014: mutations,
784 PTMs and recalibrations. Nucleic Acids Res 43: D512-520.
785 76. Thompson JD, Gibson TJ, Plewniak F, Jeanmougin F, Higgins DG (1997) The CLUSTAL_X windows
786 interface: flexible strategies for multiple sequence alignment aided by quality analysis tools.
787 Nucleic Acids Res 25: 4876-4882.
788 77. Saeed AI, Bhagabati NK, Braisted JC, Liang W, Sharov V, et al. (2006) TM4 microarray software suite.
789 Methods Enzymol 411: 134-193.
790 78. Tusher VG, Tibshirani R, Chu G (2001) Significance analysis of microarrays applied to the ionizing
791 radiation response. Proc Natl Acad Sci U S A 98: 5116-5121.
792 79. Mootha VK, Lindgren CM, Eriksson KF, Subramanian A, Sihag S, et al. (2003) PGC-1alpha-responsive
793 genes involved in oxidative phosphorylation are coordinately downregulated in human diabetes.
794 Nat Genet 34: 267-273.

795 80. Subramanian A, Tamayo P, Mootha VK, Mukherjee S, Ebert BL, et al. (2005) Gene set enrichment
796 analysis: a knowledge-based approach for interpreting genome-wide expression profiles. Proc
797 Natl Acad Sci U S A 102: 15545-15550.
798 81. Shannon P, Markiel A, Ozier O, Baliga NS, Wang JT, et al. (2003) Cytoscape: a software environment
799 for integrated models of biomolecular interaction networks. Genome Res 13: 2498-2504.
800 82. Smoot ME, Ono K, Ruscheinski J, Wang PL, Ideker T (2011) Cytoscape 2.8: new features for data
801 integration and network visualization. Bioinformatics 27: 431-432.
802 83. Martin A, Ochagavia ME, Rabasa LC, Miranda J, Fernandez-de-Cossio J, et al. BisoGenet: a new tool
803 for gene network building, visualization and analysis. BMC Bioinformatics 11: 91.
804 84. Jassal B, Matthews L, Viteri G, Gong C, Lorente P, et al. The reactome pathway knowledgebase.
805 Nucleic Acids Res 48: D498-D503.
806 85. Tabas-Madrid D, Nogales-Cadenas R, Pascual-Montano A (2012) GeneCodis3: a non-redundant and
807 modular enrichment analysis tool for functional genomics. Nucleic Acids Res 40: W478-483.
808 86. Maere S, Heymans K, Kuiper M (2005) BiNGO: a Cytoscape plugin to assess overrepresentation of
809 gene ontology categories in biological networks. Bioinformatics 21: 3448-3449.

810

811 Supporting information

812 **S1 Fig. Bidimensional clustering of most differentially expressed proteins**
813 **resulting from the analysis of proteomic data of CaCo-2 cells infected by SARS-**
814 **CoV-2 from Bojkova et al.(2020).** Horizontal axis represents samples at different time
815 points and vertical axis represent differentially expressed proteins. Rows corresponding
816 to viral Orf6 and host B23 proteins are labeled.

817 **S1 Table. N phospho-acceptor sites reported in four phosphoproteomics**
818 **studies*.**

819 **S2 Table. List of 102 phosphosites activated in at least two of the four**
820 **phosphoproteomic studies.** Level 1 (in 4 experiments), level 2 (in 3 experiments) and
821 level 3 (in 2 experiments).

822 **S3 Table. REACTOME pathways enrichment results.**

823 **S4 Table. Human phenotypes enrichment results.**

824

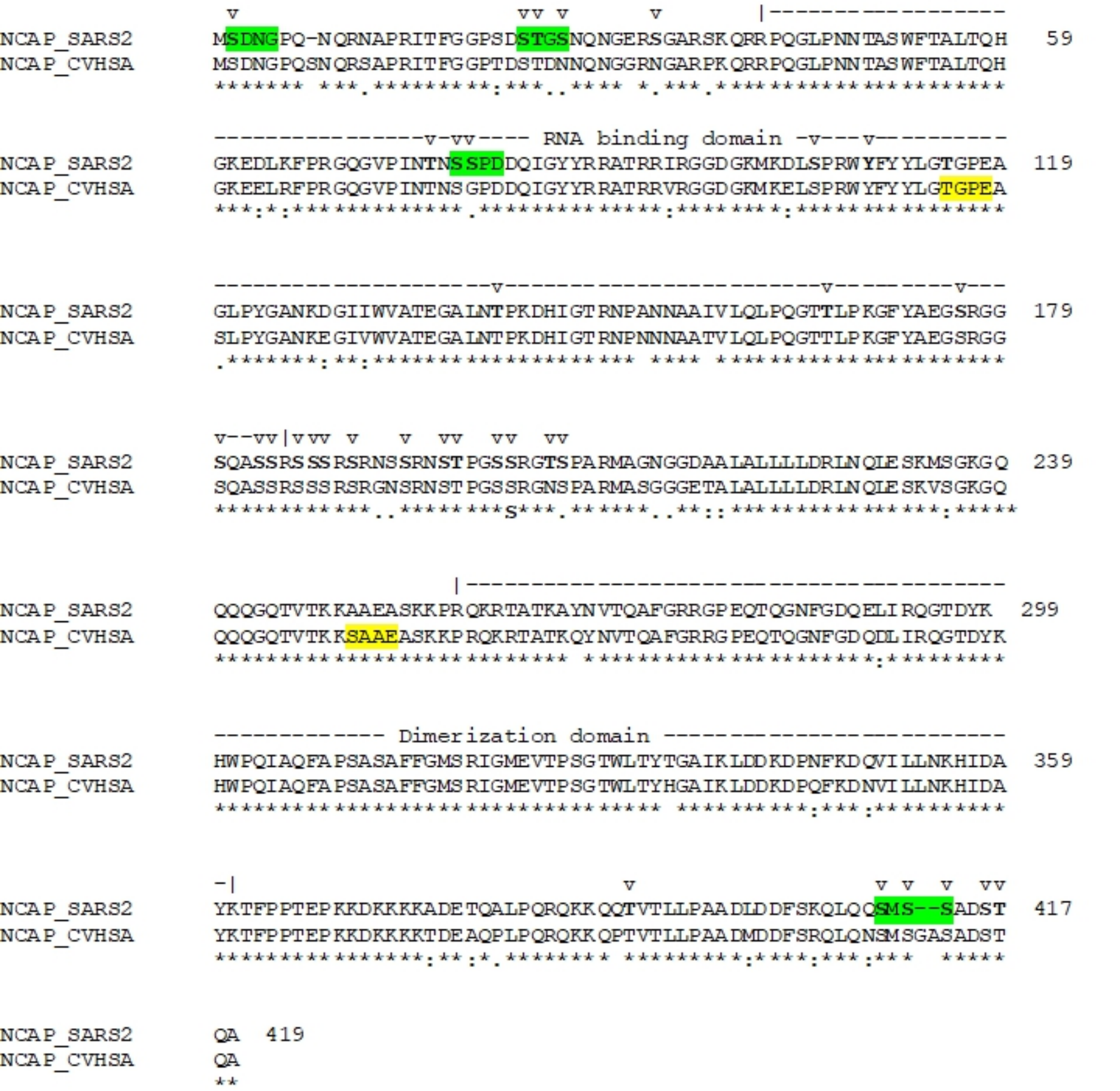
NCAP_SARS2
NCAP_CVHSA
RNA binding domain
Dimerization domain
59
119
179
239
299
359
417
419

Figure

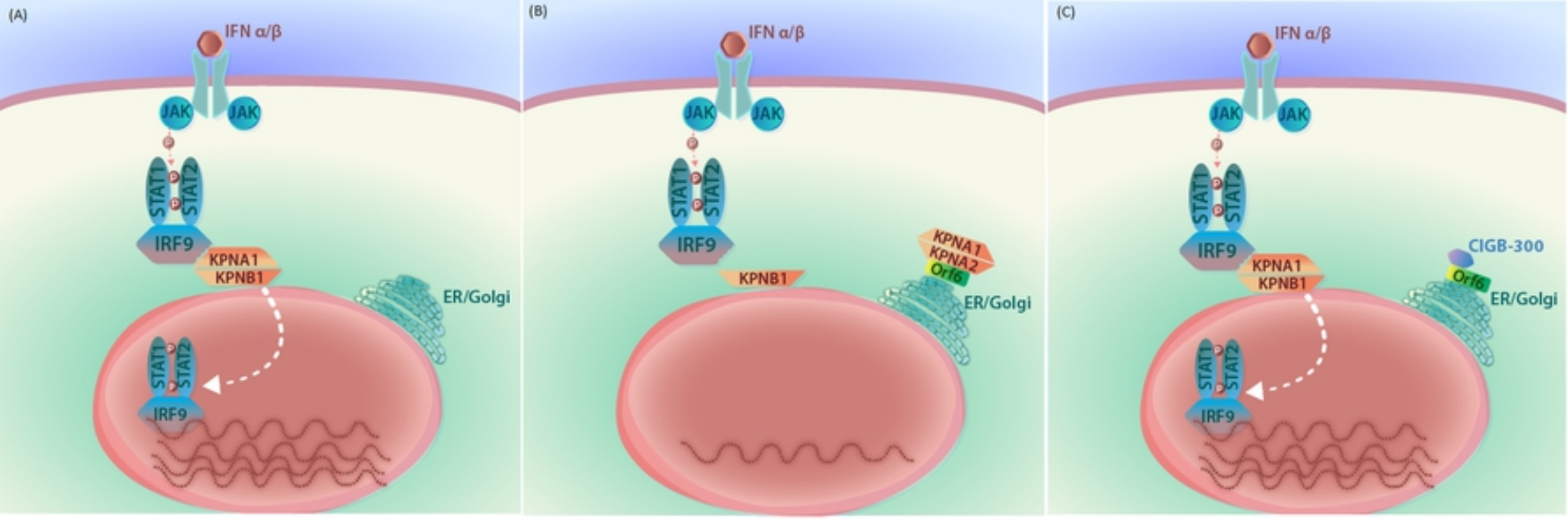
(A)
IFN α/β
JAK
JAK
P
STAT1
STAT2
IRF9
KPNA1
KPNB1
ER/Golgi
STAT1
STAT2
IRF9
(B)
IFN α/β
JAK
JAK
STAT1
STAT2
IRF9
KPNB1
KPNA1
KPNA2
Orf6
ER/Golgi
(C)
IFN α/β
JAK
JAK
STAT1
STAT2
IRF9
KPNA1
KPNB1
CIGB-300
Orf6
ER/Golgi
STAT1
STAT2
IRF9

Figure

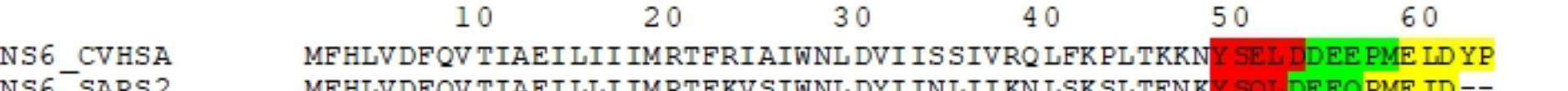
10 20 30 40 50 60
NS6_CVHSA MFHLVDFQVTIAEILIIIMRTFRIAIWNLDVIISSIVRQLFKPLTKKNYSELDDEEPMELDYP
NS6_SARS2 MFHLVDFQVTIAEILLIIMRTFKVSIWNLDYIINLIIKNLSKSLTENKYSQLDEEQPMEID--

Figure

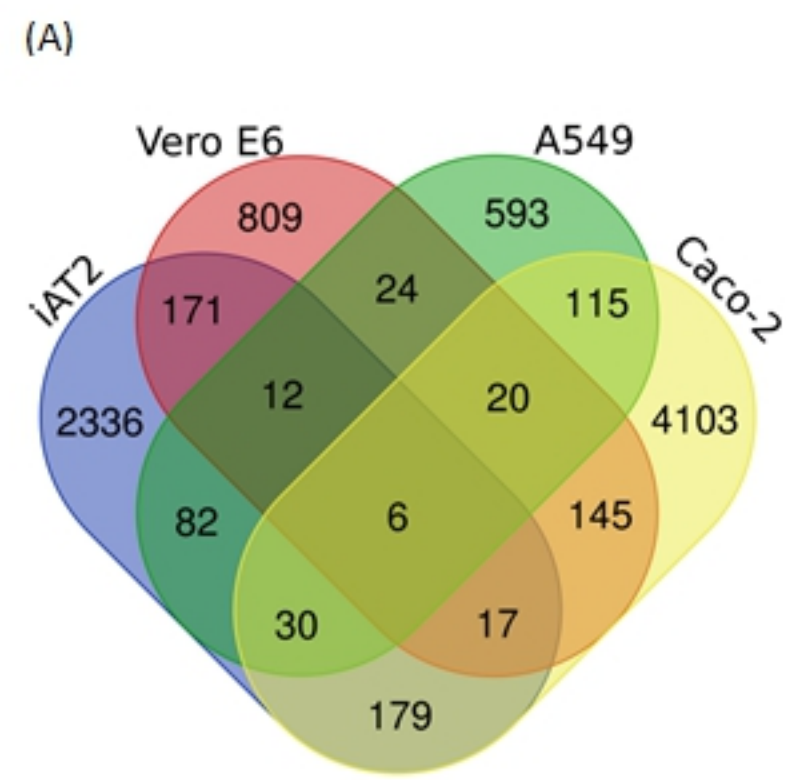
(A)
Vero E6
A549
iAT2
Caco-2
809
593
171
24
115
2336
12
20
4103
82
6
145
30
17
179

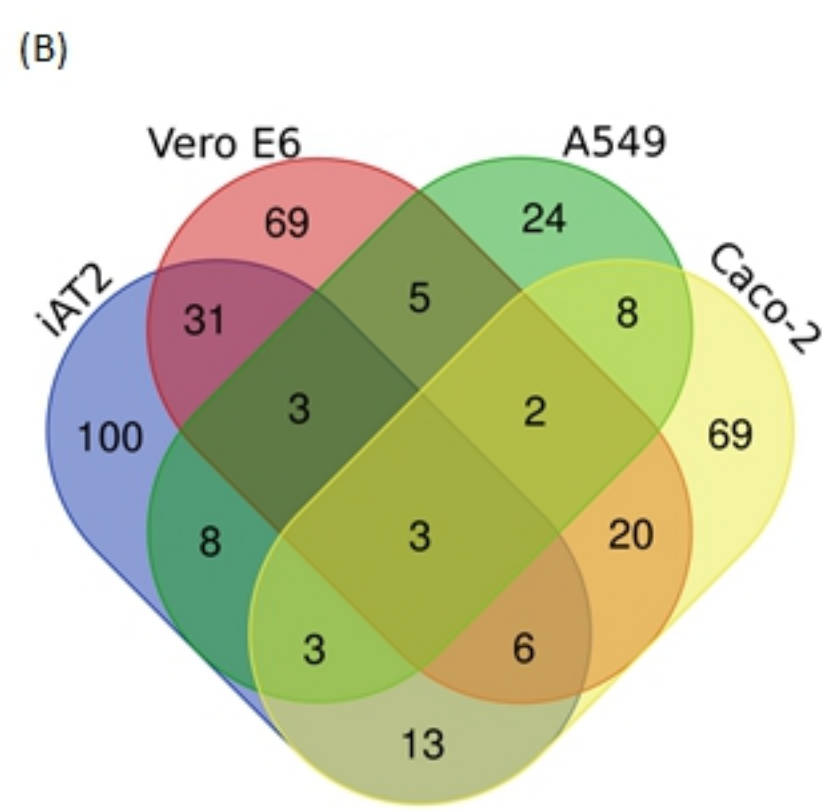
(B)
Vero E6
A549
iAT2
Caco-2
69
24
31
5
8
100
3
2
69
8
3
20
3
6
13

Figure

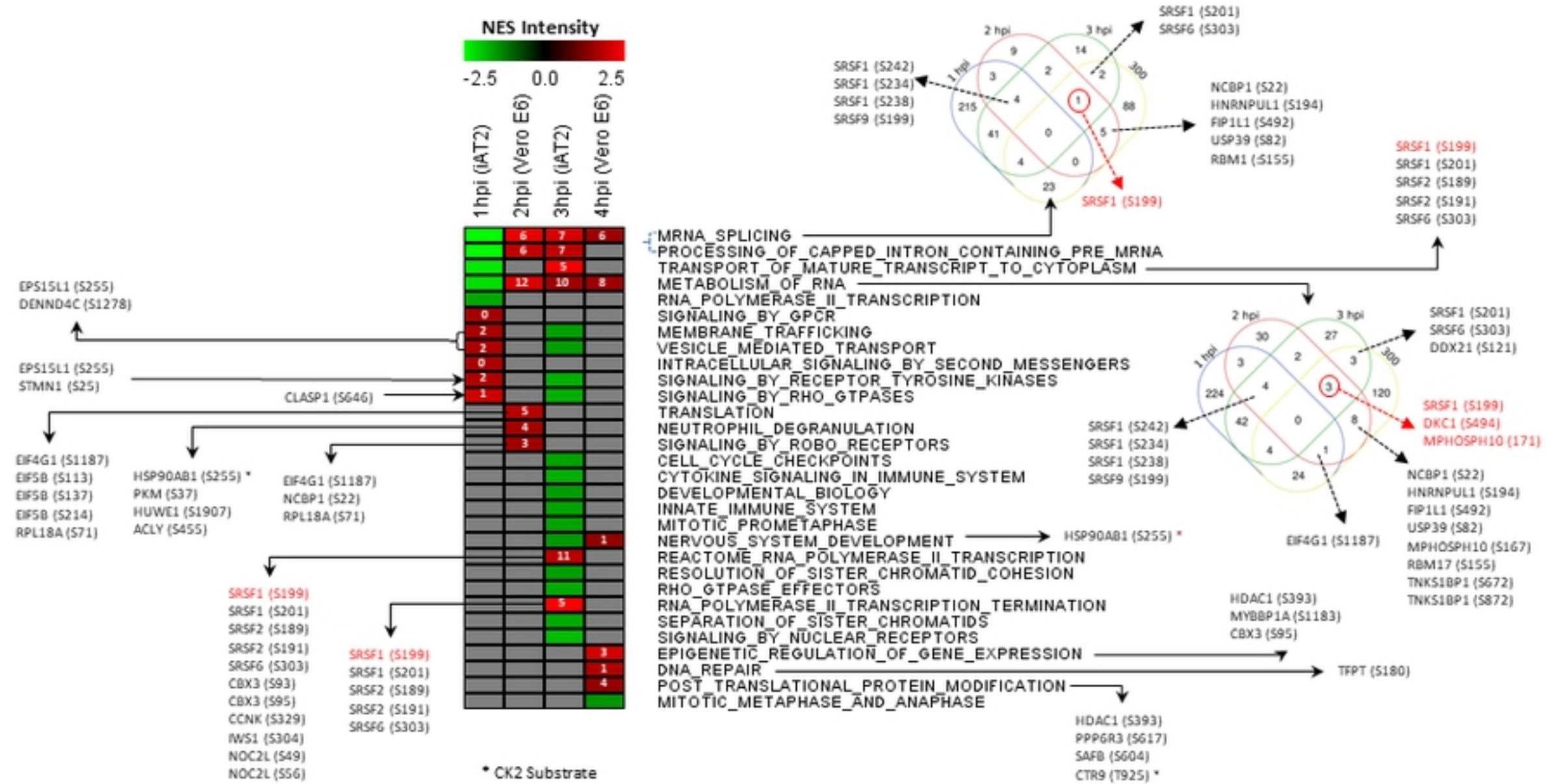
NES Intensity
-2.5
0.0
2.5
1hpi (iAT2)
2hpi (Vero E6)
3hpi (iAT2)
4hpi (Vero E6)
MRNA_SPLICING
PROCESSING_OF_CAPPED_INTRON_CONTAINING_PRE_MRNA
TRANSPORT_OF_MATURE_TRANSCRIPT_TO_CYTOPLASM
METABOLISM_OF_RNA
RNA_POLYMERASE_II_TRANSCRIPTION
SIGNALING_BY_GPCR
MEMBRANE_TRAFFICKING
VESICLE_MEDIATED_TRANSPORT
INTRACELLULAR_SIGNALING_BY_SECOND_MESSENGERS
SIGNALING_BY_RECEPTOR_TYROSINE_KINASES
SIGNALING_BY_RHO_GTPASES
TRANSLATION
NEUTROPHIL_DEGRANULATION
SIGNALING_BY_ROBO_RECEPTORS
CELL_CYCLE_CHECKPOINTS
CYTOKINE_SIGNALING_IN_IMMUNE_SYSTEM
DEVELOPMENTAL_BIOLOGY
INNATE_IMMUNE_SYSTEM
MITOTIC_PROMETAPHASE
NERVOUS_SYSTEM_DEVELOPMENT
REACTOME_RNA_POLYMERASE_II_TRANSCRIPTION
RESOLUTION_OF_SISTER_CHROMATID_COHESION
RHO_GTPASE_EFFECTORS
RNA_POLYMERASE_II_TRANSCRIPTION_TERMINATION
SEPARATION_OF_SISTER_CHROMATIDS
SIGNALING_BY_NUCLEAR_RECEPTORS
EPIGENETIC_REGULATION_OF_GENE_EXPRESSION
DNA_REPAIR
POST_TRANSLATIONAL_PROTEIN_MODIFICATION
MITOTIC_METAPHASE_AND_ANAPHASE
EPS15L1 (S255)
DENND4C (S1278)
EPS15L1 (S255)
STMN1 (S25)
CLASP1 (S646)
EIF4G1 (S1187)
EIF5B (S113)
EIF5B (S137)
EIF5B (S214)
RPL18A (S71)
HSP90AB1 (S255) *
PKM (S37)
HUWE1 (S1907)
ACLY (S455)
EIF4G1 (S1187)
NCBP1 (S22)
RPL18A (S71)
SRSF1 (S199)
SRSF1 (S201)
SRSF2 (S189)
SRSF2 (S191)
SRSFG (S303)
CBX3 (S93)
CBX3 (S95)
CCNK (S329)
IWS1 (S304)
NOC2L (S49)
NOC2L (S56)
SRSF1 (S199)
SRSF1 (S201)
SRSF2 (S189)
SRSF2 (S191)
SRSFG (S303)
* CK2 Substrate
2 hpi
3 hpi
1 hpi
SRSF1 (S242)
SRSF1 (S234)
SRSF1 (S238)
SRSF9 (S199)
SRSF1 (S201)
SRSFG (S303)
NCBP1 (S22)
HNRNPUL1 (S194)
FIP1L1 (S492)
USP39 (S82)
RBM1 (S155)
SRSF1 (S199)
SRSF1 (S199)
SRSF1 (S201)
SRSF2 (S189)
SRSF2 (S191)
SRSFG (S303)
2 hpi
3 hpi
1 hpi
SRSF1 (S242)
SRSF1 (S234)
SRSF1 (S238)
SRSF9 (S199)
SRSF1 (S201)
SRSFG (S303)
DDX21 (S121)
SRSF1 (S199)
DKC1 (S494)
MPHOSPH10 (171)
NCBP1 (S22)
HNRNPUL1 (S194)
FIP1L1 (S492)
USP39 (S82)
MPHOSPH10 (S167)
RBM17 (S155)
TNKS1BP1 (S672)
TNKS1BP1 (S872)
HSP90AB1 (S255) *
EIF4G1 (S1187)
HDAC1 (S393)
MYBBP1A (S1183)
CBX3 (S95)
TFPT (S180)
HDAC1 (S393)
PPP6R3 (S617)
SAFB (S604)
CTR9 (T925) *

Figure

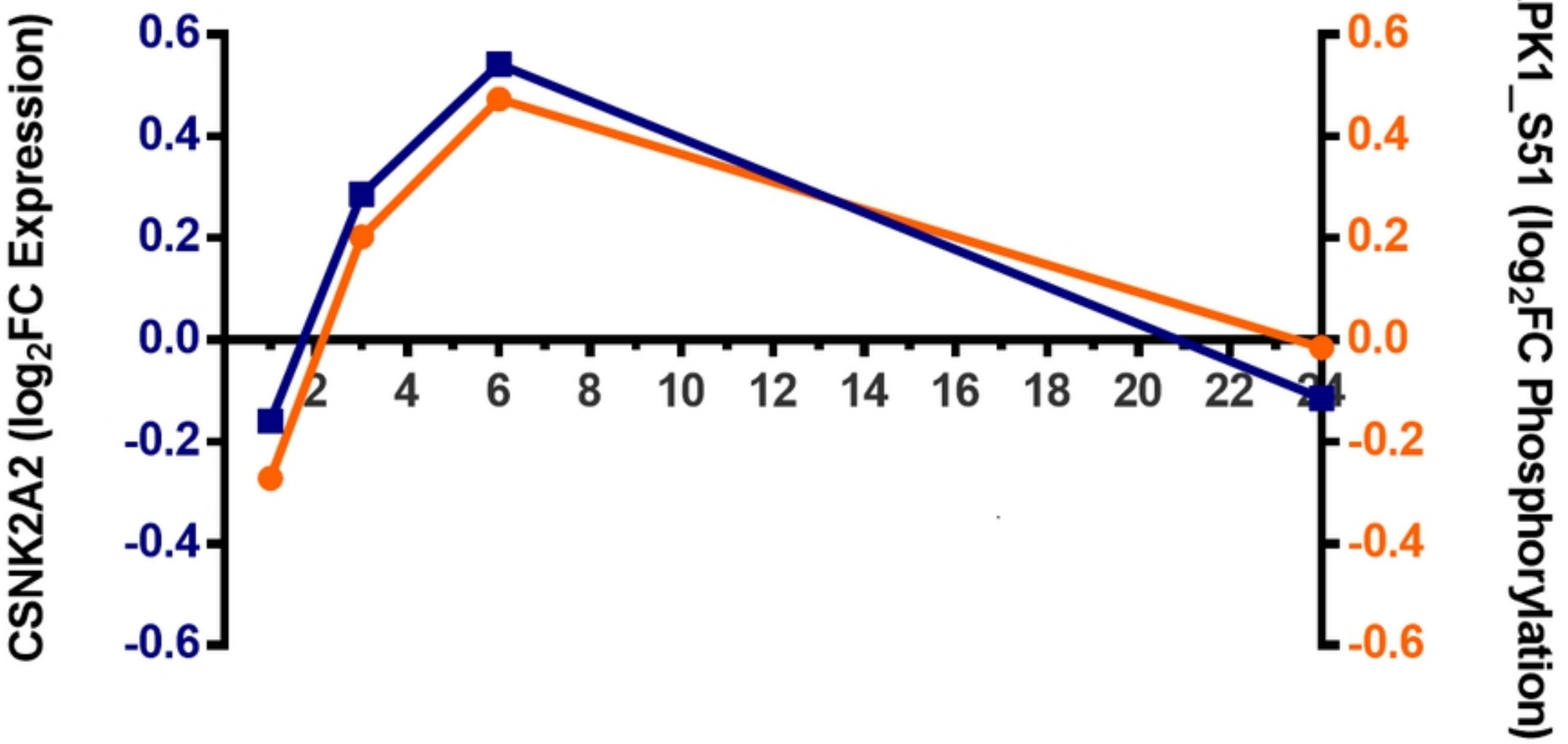
CSNK2A2 (log2FC Expression)
SRPK1_S51 (log2FC Phosphorylation)
0.6
0.4
0.2
0.0
-0.2
-0.4
-0.6
2
4
6
8
10
12
14
16
18
20
22

Figure

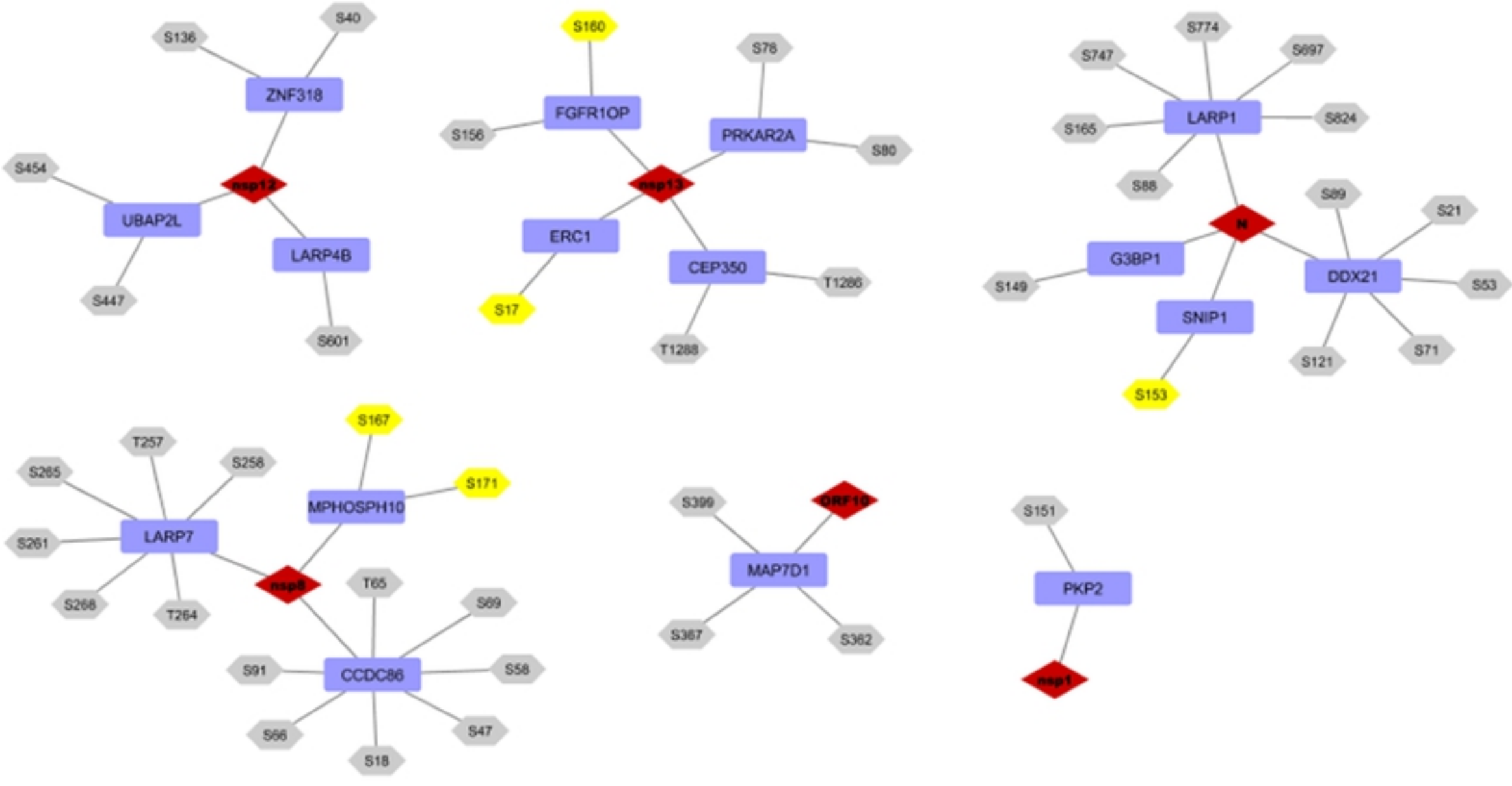
S40
S136
ZNF318
S454
nsp12
UBAP2L
LARP4B
S447
S601
S160
S76
FGFR1OP
S156
PRKAR2A
S80
nsp13
ERC1
CEP350
T1286
S17
T1288
S774
S747
S697
LARP1
S165
S824
S88
S89
S21
N
G3BP1
DDX21
S149
S53
SNIP1
S71
S121
S153
S167
T257
S258
S265
MPHOSPH10
S171
S261
LARP7
nsp8
T65
S69
S268
T264
S91
CCDC86
S58
S66
S47
S18
S399
ORF10
MAP7D1
S367
S362
S151
PKP2
nsp1

Figure

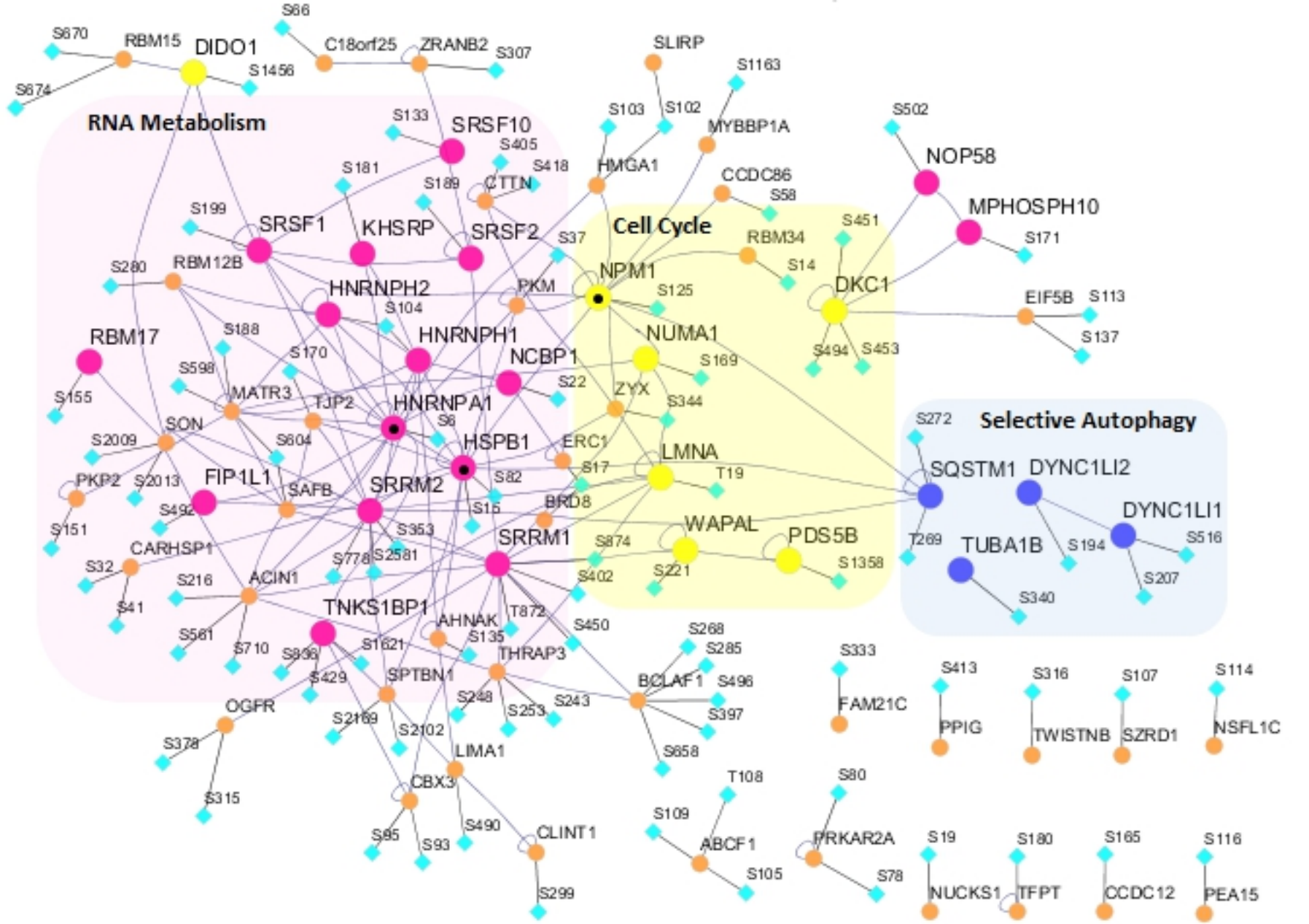
RNA Metabolism
Cell Cycle
Selective Autophagy
DIDO1
RBM15
C18orf25
ZRANB2
SRSF10
SRSF1
KHSRP
SRSF2
RBM12B
HNRNPH2
HNRNPH1
RBM17
MATR3
TJP2
HNRNPA1
SON
HSPB1
FIP1L1
SAFB
SRRM2
CARHSP1
ACIN1
SRRM1
TNKS1BP1
AHNAK
THRAP3
SPTBN1
OGFR
LIMA1
CBX3
CLINT1
CTTN
HMGA1
SLIRP
MYBBP1A
NPM1
PKM
NUMA1
NCBP1
ZYX
ERC1
LMNA
BRD8
WAPAL
PDS5B
CCDC86
RBM34
DKC1
NOP58
MPHOSPH10
EIF5B
SQSTM1
DYNC1LI2
DYNC1LI1
TUBA1B
BCLAF1
FAM21C
PPIG
TWISTNB
SZRD1
NSFL1C
ABCF1
PRKAR2A
NUCKS1
TFPT
CCDC12
PEA15

Figure

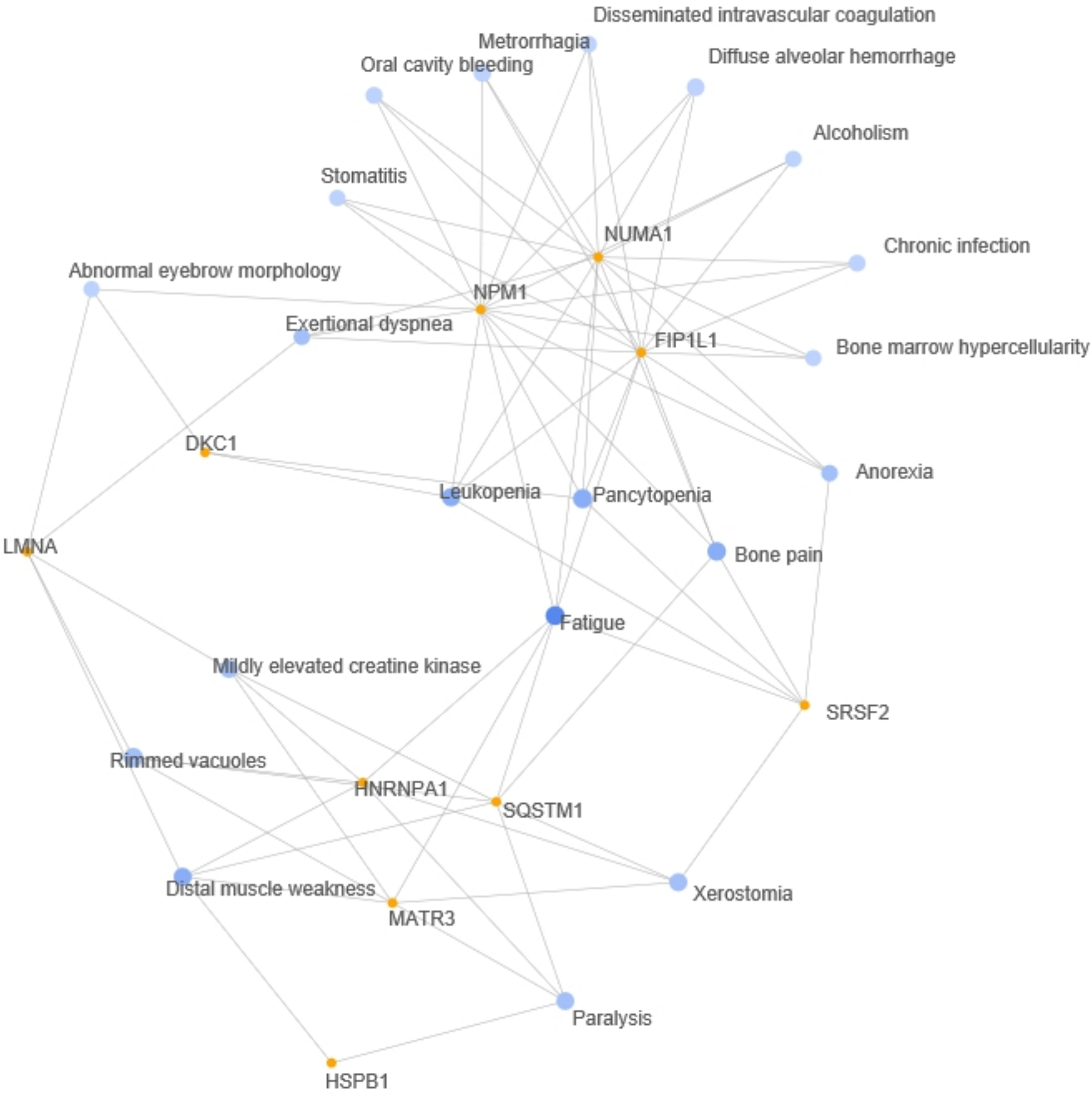
Disseminated intravascular coagulation
Metrorrhagia
Oral cavity bleeding
Diffuse alveolar hemorrhage
Alcoholism
Stomatitis
NUMA1
Chronic infection
Abnormal eyebrow morphology
NPM1
Exertional dyspnea
FIP1L1
Bone marrow hypercellularity
DKC1
Anorexia
Leukopenia
Pancytopenia
LMNA
Bone pain
Fatigue
Mildly elevated creatine kinase
SRSF2
Rimmed vacuoles
HNRNPA1
SQSTM1
Distal muscle weakness
Xerostomia
MATR3
Paralysis
HSPB1

Figure